THE JOURNAL OF BIOLOGICAL CHEMISTRY VOL. 284, NO. 28, pp. 19067–19076, July 10, 2009

An *ab Initio* Structural Model of a Nucleoside Permease Predicts Functionally Important Residues*[S]

Received for publication, February 20, 2009, and in revised form, May 6, 2009 Published, JBC Papers in Press, May 8, 2009, DOI 10.1074/jbc.M109.017947

Raquel Valdés[‡], Shirin Arastu-Kapur[§1], Scott M. Landfear[‡2], and Ujwal Shinde[§3]

From the Departments of [‡]Molecular Microbiology and Immunology and [§]Biochemistry and Molecular Biology, Oregon Health & Science University, Portland, Oregon 97239

Permeases belonging to the equilibrative nucleoside transporter family promote uptake of nucleosides and/or nucleobases into a wide range of eukaryotes and mediate the uptake of a variety of drugs used in the treatment of cancer, heart disease, AIDS, and parasitic infections. No experimental three-dimensional structure exists for any of these permeases, and they are not present in prokaryotes, the source of many membrane proteins used in crystal structure determination. To generate a structural model for such a transporter, the LdNT1.1 nucleoside permease from the parasitic protozoan *Leishmania donovani* was modeled using *ab initio* computation. Site-directed mutations that strongly impair transport or that alter substrate specificity map to the central pore of the *ab initio* model, whereas mutations that have less pronounced phenotypes map to peripheral positions. The model suggests that aromatic residues present in transmembrane helices 1, 2, and 7 may interact to form an extracellular gate that closes the permeation pathway in the inward oriented conformation. Mutation of two of these three residues abrogated transport activity, consistent with the prediction of the model. The *ab initio* model is similar to one derived previously using threading analysis, a distinct computational approach, supporting the overall accuracy of both models. However, significant differences in helix orientation and residue position between the two models are apparent, and the mutagenesis data suggest that the *ab initio* model represents an improvement regarding structural details over the threading model. The putative gating interaction may also help explain differences in substrate specificity between members of this family.

Nucleoside transporters play pivotal roles in nucleoside salvage pathways, regulation of adenosine signaling, and the pharmacology of antineoplastic and antiviral nucleoside drugs (1, 2). Salvage of nucleosides and nucleobases is the first step of nucleoside utilization in those cells that lack the metabolic machinery to make purine nucleotides *de novo*, including protozoan parasites (3) and brain and bone marrow cells in mammals (4). Nucleoside permeases also mediate the uptake of a number of nucleoside analog drugs used to combat the devastating effects of chronic diseases, including those caused by RNA viruses, cancer, and parasitic protozoan infections (5, 6).

Equilibrative nucleoside transporters (ENTs)[4] are a unique family of proteins (the SLC29 family), with no apparent sequence homology to other types of permeases, that enable facilitated diffusion of nucleosides, nucleoside analogs, and nucleobases across cell membranes. Although widely distributed among eukaryotes from protozoa to humans, ENT-like homologs have not been identified in prokaryotes, and therefore crystallization of these transporters is likely to be even more challenging than for those membrane proteins that do have orthologs in prokaryotes. In the absence of a crystallographic structure, the use of genetic and biochemical approaches, especially site-directed mutagenesis, has begun to reveal a significant number of elements involved in ENT function (7–23). Previous studies on the LdNT1.1 adenosine and pyrimidine nucleoside permease from the parasitic protozoan *Leishmania donovani*, an organism that cannot synthesize purines *de novo* and relies upon purine uptake for survival, have led to valuable insights into the structure and function of this family of permeases (9, 13, 22). Nevertheless, structural coverage is still sparse, and the functional determinants within the ENTs that control substrate translocation and specificity remain largely unknown.

Emerging computational methods to overcome the paucity of high resolution structural data include the development of models based upon *ab initio* techniques (24–26) and fold recognition or "threading" (27). *Ab initio* techniques utilize the physical properties of the primary amino acid sequence to predict structures, whereas threading methods search for an optimal fit of the query sequence onto known three-dimensional structures of other proteins. A preliminary three-dimensional topology for the LdNT2 inosine/guanosine/xanthosine transporter from *L. donovani* was generated using threading analysis upon the template of the structurally resolved glycerol-3-phosphate transporter of *E. coli* (12), and a similar threading analysis revealed structural similarities between the TbNT1 nucleobase

* This work was supported, in whole or in part, by National Institutes of Health Grant AI44138 (to S. M. L.). This work was also supported by National Science Foundation Grant 0746589 (to U. S.).

[S] The on-line version of this article (available at http://www.jbc.org) contains supplemental Figs. S1 and S2.

[1] Present address: Proteolix, Inc., 333 Allerton Ave., South San Francisco, CA 94080.

[2] To whom correspondence may be addressed: Dept. of Molecular Microbiology and Immunology, Oregon Health & Science University, 3181 S.W. Sam Jackson Park Rd., Portland, OR 97239. Tel.: 503-494-2426; Fax: 503-494-6862; E-mail: landfear@ohsu.edu.

[3] To whom correspondence may be addressed: Dept. of Biochemistry and Molecular Biology, Oregon Health & Science University, 3181 S.W. Sam Jackson Park Rd., Portland, OR 97239. Tel.: 503-494-8683; Fax: 503-494-8393; E-mail: shindeu@ohsu.edu.

[4] The abbreviations used are: ENT, equilibrative nucleoside transporter; LdNT, *L. donovani* nucleoside transporter; TbNBT, *T. brucei* nucleobase transporter; TM, transmembrane; GFP, green fluorescent protein.

transporter of *Trypanosoma brucei* and the lactose permease of *E. coli* (28). In the current study, we have used a distinct computational approach based upon *ab initio* algorithms (24) in conjunction with site-directed mutagenesis to arrive at a structural model for LdNT1.1. An encouraging outcome is that both the *ab initio* and threading approaches resulted in two structural models that share the same overall topology. However, the *ab initio* model provided structural and functional details not previously observed in the threading model. Indeed, experiments based upon the *ab initio* model led to the identification of eight new residues that moderately affected LdNT1.1 activity and six novel residues whose mutation abrogated transport function. Most notably, the *ab initio* model revealed two aromatic amino acids (Phe^{48} in TM1 and Trp^{75} in TM2) that may form an interaction motif located in the pore and be involved in holding the transporter in the inward-open conformation. Mutagenesis of these residues confirmed that they are essential for transport. Therefore, the *ab initio* model of LdNT1.1 offers a framework for predicting intramolecular interactions central to the function of this and related nucleoside permeases.

EXPERIMENTAL PROCEDURES

Chemicals, Materials, and Reagents—Restriction endonucleases and DNA-modifying enzymes were obtained from New England Biolabs, Inc., Roche Applied Science, or Invitrogen. Radiolabeled [2,8-^{3}H]adenosine (50 Ci/mmol), [5,6-^{3}H]uridine (32.3 Ci/mmol), [8-^{3}H]guanosine (5.6 Ci/mmol), [2,8-^{3}H]-inosine (39 Ci/mmol), [2,8-^{3}H]adenine (27 Ci/mmol), [5,6-^{3}H]uracil (43.3 Ci/mmol), [8-^{3}H]guanine (7.6 Ci/mmol), and [8-^{3}H]xanthine (12.8 Ci/mmol) were purchased from Moravek Biochemicals. All other chemicals, materials, and reagents were of the highest commercial quality available.

Parasite Cell Cultures—L. donovani strains were propagated at 26 °C in RPMI medium (Invitrogen) containing 10% fetal bovine serum, 15 μg/ml hemin, and 100 μM xanthine. Null mutants Δ*ldnt1* and Δ*ldnt1*/Δ*ldnt2* (29) were supplemented with drugs against the integrated resistance markers (50 μg/ml hygromycin (Roche Applied Science) or 50 μg/ml hygromycin plus 50 μg/ml phleomycin (Research Products International), respectively) as well as drugs that are cytotoxic to parasites expressing the wild type LdNT1.1 or LdNT2 transporters (1 μM tubercidin (Sigma-Aldrich) or 1 μM formycin B (Berry & Associates), respectively). Parasites transfected with pX63NeoRI or pXG-GFP+2′ constructs (described below) were selected and maintained in 100 μg/ml G418 (Invitrogen).

Site-directed Mutagenesis and Plasmid Constructs—Mutagenesis was performed using the QuikChange® II XL site-directed mutagenesis kit, a polymerase chain reaction-based mutagenesis strategy (Stratagene). Mutagenic primers were designed to incorporate the desired mutation within the *LdNT1.1* open reading frame template that had been ligated into the EcoRI site of the episomal expression vector pX63NeoRI (13). The codons used to introduce the point mutations are listed: M40A (ATG → GCG); M40D (ATG → GAT); F48A (TTC → GCC); W75A (TGG → GCG); S90T (AGC → ACC); P95A (CCG → GCG); T97S, T344S, and T475S (ACG → TCG); L118A (CTG → GCG); I122A (ATC → GCC); G149A (GGC → GCC); E157D (GAG → GAT); E157Q (GAG → CAG); V179A (GTC → GCC); S187T (TCG → ACG); Q190N (CAG → AAC); N340Q (AAT → CAG); F341A (TTT → GCT); L342A (CTC → GCC); F346A (TTC → GCC); N436Q (AAC → CAG); G440A (GGC → GCC); G440F (GGC → TTC); L471I (CTC → ATC); S469F (TCC → TTC) T478S (ACC → AGC); and T478F (ACC → TTC). For each mutant, two independent clones were isolated in parallel. The presence of mutations was verified by DNA sequencing at the Oregon Health & Science University Microbiology Research Core Facility using a model 377 Applied Biosystems automated fluorescence sequencer (PerkinElmer Life Sciences). Mutant clones were transfected into the transport-defective Δ*ldnt1*/Δ*ldnt2 L. donovani* cell line as described below. To generate GFP fusions at the amino terminus of LdNT1.1 (GFP-LdNT1.1), open reading frames of the wild type and mutated *LdNT1.1* genes were amplified by PCR using forward and reverse primers containing BamHI restriction sites. After restriction digestion, the open reading frames were subcloned into the BamHI site of the pXG-GFP+2′ vector (30). Mutant clones were selected by PCR screening and restriction enzyme mapping, and mutations were confirmed again by DNA sequencing before being transfected into the Δ*ldnt1 L. donovani* cell line.

Cell Transfection into Leishmania and Selection of Stable Transfectants—Wild type and mutant *LdNT1.1* pX63NeoRI and pXG-GFP+2′ constructs were transfected into transport defective Δ*ldnt1*/Δ*ldnt2* and Δ*ldnt1 L. donovani* promastigotes, respectively, using standard electroporation conditions (31, 32). Transfectants were selected and expanded in liquid medium containing 100 μg/ml G418.

Transport Assays—L. donovani promastigotes expressing the wild type LdNT1.1 transporter and the mutant permeases were harvested between early and mid-log phases, washed three times in phosphate-buffered saline (138 mM NaCl, 8.1 mM $Na_2HPO_4{\cdot}7H_2O$, 2.7 mM KCl, 1.5 mM KH_2PO_4, pH 7.4), and resuspended in phosphate-buffered saline to a final density of $2–3 \times 10^8$ parasites/ml. Nucleoside transport measurements were performed in triplicate for 30 s using 100-μl aliquots by the previously described oil stop method (33). Wild type and mutant *LdNT1.1* pX63NeoRI transfectants were screened for nucleoside and nucleobase uptake under the following conditions: Ado (1 μM, 1 μCi/ml), Urd (5 μM, 2 μCi/ml), Guo (10 μM, 10 μCi/ml), Ino (10 μM, 10 μCi/ml), Ade (25 μM, 2.5 μCi/ml), Ura (25 μM, 2.5 μCi/ml), Gua (25 μM, 2.5 μCi/ml), and Xan (25 μM, 2.5 μCi/ml).

Fluorescence Microscopy—Fluorescence microscopy of logarithmic phase promastigotes was performed as described previously (9). The slides were observed under a 60× oil immersion lens with a Nikon Microphot-FX phase contrast microscope, and the images were captured using MagnaFire software (Optronics).

Ab Initio Modeling and Docking Analysis—Structural models for the *L. donovani* LdNT1.1 nucleoside transporter were constructed using Rosetta *ab initio* modeling software (24–26). Briefly, structure fragments were generated using the standard Rosetta fragment server and employing only the SAM-T99 secondary structure prediction method during the fragment selection procedure. Five thousand independent simulations were generated and were subjected to clustering analysis. The cen-

ters of the three largest clusters were chosen as the three best models, defined as having the lowest standard deviation of the mean among positions of α-carbon atoms of all residues to all other simulations in a cluster. All of the models showed a similar overall topology for the membrane spanning regions and were consistent with TM region predictions using TMPred and MEMSAT2 (34). These models were also compared with an LdNT1.1 structural model derived using threading analysis, as previously described for LdNT2 (12). The best *ab initio* prediction, as defined by consistency with results of site-directed mutagenesis, and the threading model were then allowed to dock with the natural substrate adenosine using Patchdock.

RESULTS

Ab Initio Model of LdNT1.1—To provide insight into the structure and function of an ENT family member, an *ab initio* structural model was developed for LdNT1.1, a nucleoside transporter that has been the object of significant mutagenesis studies (9, 13, 22). Analysis of LdNT1.1 using Rosetta software yielded three simulations for the helical bundling and putative substrate permeation pore of the transporter (Fig. 1*A*). In these models, the predicted positions of TM helices are shown as rigid cylinders, but the structures of the hydrophilic loops connecting TM helices are not displayed. These three models were then evaluated experimentally by generating a battery of site-directed mutants (Table 1) and determining the functional properties of each mutant.

To validate the *ab initio* approach to modeling membrane transporters, we also employed Rosetta software to compute a structural model for the lactose permease from *E. coli*, LacY, a protein whose crystal structure has been resolved by x-ray crystallography (28). As demonstrated in supplemental Fig. S1, the *ab initio* model for LacY agreed well with the crystal structure when the disposition of the 12 transmembrane helices was compared. Upon comparing the two structures using the program PyMOL, the root mean square deviation for positions of Cα carbon atoms was 4.5 Å. This control computational exercise demonstrates the validity of employing *ab initio* modeling to derive reasonable structural models for polytopic membrane proteins.

Selection of Candidate Amino Acid Residues for Site-directed Mutagenesis—The evaluation of the TM folding and putative nucleoside permeation cavity for each of the models described above allowed the prediction of new residues whose modification might strongly impair transport activity because of their localization within the predicted pore of at least one of the three models (Met^{40}, TM1; Pro^{95}, TM2; Leu^{118} and Ile^{122}, TM3; Glu^{157}, edge of TM4; Phe^{341} and Leu^{342}, TM7; Gly^{440}, TM10; and Ser^{469} and Thr^{478}, TM11). The additional amino acids targeted included residues located within the same helical faces as residues previously described to affect solute translocation or amino acids within amphipathic helices predicted to line the pore by threading analysis (12) (Ser^{90} and Thr^{97}, TM2; Gly^{149}, TM4; Val^{179}, Ser^{187}, and Gln^{190}, TM5; Asn^{340} and Thr^{344}, TM7; Asn^{436}, TM10; Leu^{471} and Thr^{475}, TM11). As a result of this exercise, 21 candidate amino acids were selected to further examine LdNT1.1 function by site-directed mutagenesis (Table 1). Conservative replacements were undertaken in many cases, because they often lead to changes in substrate specificity (9, 22). However, for some residues, nonconservative substitutions (M40A, M40D, P95A, L118A, I122A, F341A, L342A, G440F, S469F, and T478F) or replacements that abrogate the charge of the original residue (E157Q) were also introduced and evaluated.

Functional Characterization of LdNT1.1 Mutants—To assess the functional roles in ligand permeation of the candidate residues, the mutant permeases were expressed in the transport-defective Δ*ldnt1*/Δ*ldnt2 L. donovani* double knockout cell line that is genetically deficient in the *LdNT1.1*, *LdNT1.2*, and *LdNT2* genes and consequently provides a null background for transport of nucleosides (29). The ability of each mutant permease to mediate ligand translocation was evaluated by uptake assays using 1 μM [^{3}H]adenosine and 5 μM [^{3}H]uridine, both natural substrates of LdNT1.1. Mutations of six residues (M40D in TM1, E157Q and E157D in the edge of predicted TM4, F341A in TM7, G440F in TM10, and S469F and T478F in TM11) virtually abrogated transport capability (loss of >95% activity *versus* the wild type) for at least one ligand (Fig. 2*A*). These mutations were designated "crippled" for transport function (Table 2). Notably, mutations E157D and F341A resulted in permeases that were capable of transporting adenosine, albeit at lower rates (~15–25% of residual activity *versus* the wild type) but exhibited no detectable uptake of uridine, indicating that they had undergone a change in substrate specificity. In addition, M40A in TM1, S90T in TM2, V179A and S187T in TM5, N340Q and T344S in TM7, N436Q and G440A in TM10, and T478S in TM11 (Fig. 2*B*) also resulted in substantial inhibition of activity that varied from ~50 to ~75% *versus* the wild type. Although these mutants did not display crippling phenotypes, it is possible that further detailed kinetic studies could provide useful information for structure-function analysis. The remaining nine mutants did not show significant differences in adenosine or uridine uptake when compared with the wild type transporter (data not shown).

Screening for Additional Possible Alterations in Substrate Specificity by the Mutant Permeases—The effects of mutations on permeant selectivity were evaluated by comparing uptake by mutant and wild type LdNT1.1 of a panel of radiolabeled nucleosides and nucleobases that are not natural substrates of LdNT1.1. The ability of each mutant permease to mediate ligand translocation was assessed at concentrations of 10 μM [^{3}H]inosine and [^{3}H]guanosine or 25–50 μM [^{3}H]adenine, [^{3}H]uracil, [^{3}H]guanine, and [^{3}H]xanthine. These concentrations are all above the K_m values reported for wild type nucleoside (LdNT1.1 (33) and LdNT2 (35)) and nucleobase (LmaNT3 (36)) transporters. The Δ*ldnt1*/Δ*ldnt2* double null mutant cell line provided an ideal homologous system for evaluating potential gain-of-function transport activity for inosine or guanosine, both natural ligands of LdNT2. However, Δ*ldnt1*/Δ*ldnt2* retains functional purine nucleobase transporters, and therefore the potential gain-of-function transport activity for any of the nucleobases tested had to be inferred after subtracting the inherent background measured in the Δ*ldnt1*/Δ*ldnt2* double null mutant. No significant gain-of-function differences in substrate specificity were observed in any case, when compared with the LdNT1.1 wild type (data not shown).

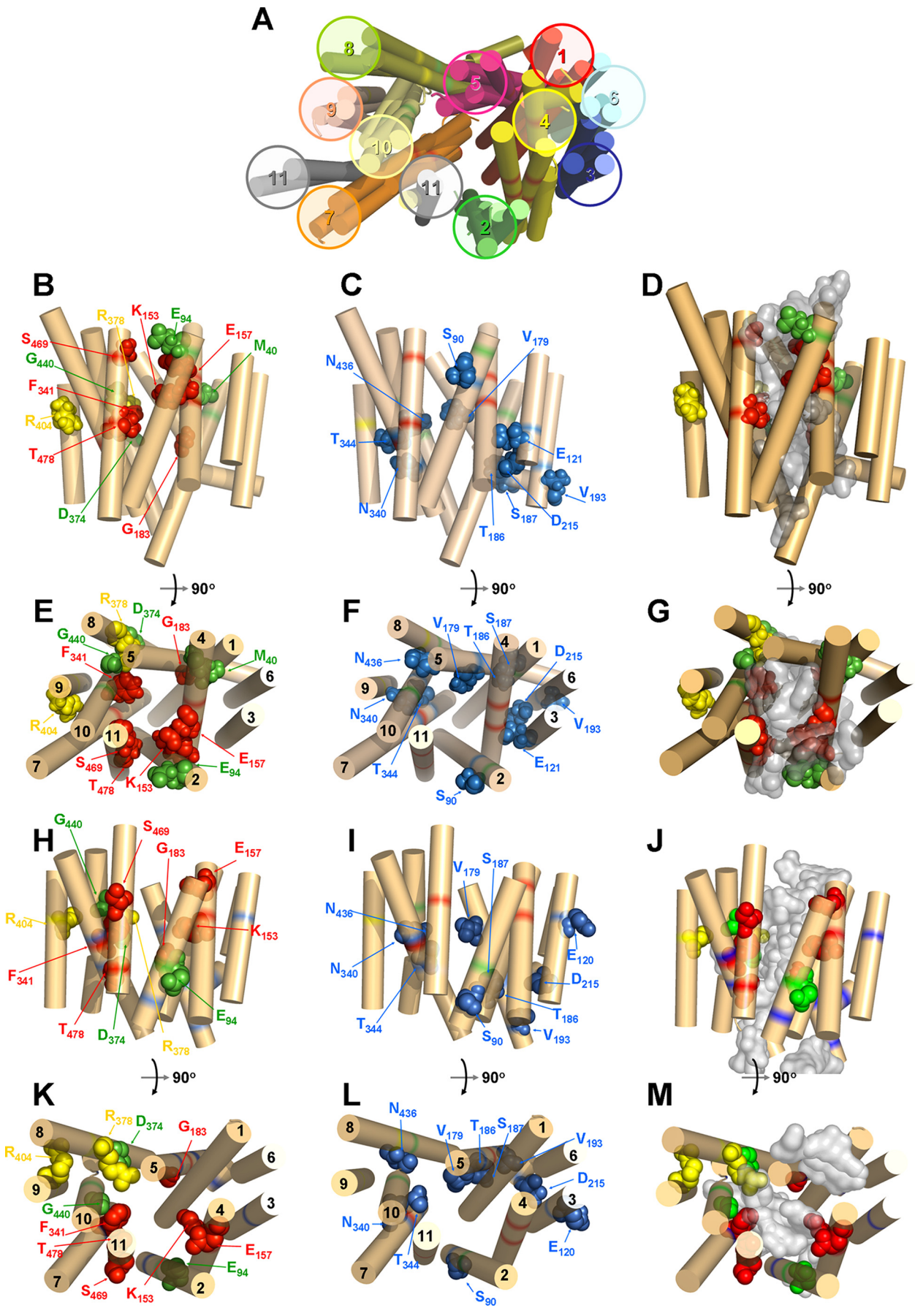
A
B
C
D
E
F
G
H
I
J
K
L
M
90°
90°
90°
90°
90°
R378
K153
E94
E157
M40
S469
G440
F341
R404
T478
D374
G183
S90
V179
N436
T344
E121
V193
N340
S187
D215
T186
E120

TABLE 1
New mutations introduced into LdNT1.1

Residue	TM domain	Mutation(s)
Met^{40}	1	M40A and M40D
Phe^{48}	1	F48A, F48Y, F48W
Trp^{75}	2	W75A, W75F, W75Y
Ser^{90}	2	S90T
Pro^{95}	2	P95A
Thr^{97}	2	T97S
Leu^{118}	3	L118A
Ile^{122}	3	I122A
Gly^{149}	4	G149A
Glu^{157}	4/edge	E157D and E157Q
Val^{179}	5	V179A
Ser^{187}	5	S187T
Gln^{190}	5	Q190N
Asn^{340}	7	N340Q
Phe^{341}	7	F341A
Leu^{342}	7	L342A
Thr^{344}	7	T344S
Asn^{436}	10	N436Q
Gly^{440}	10	G440A and G440F
Ser^{469}	11	S469F
Leu^{471}	11	L471I
Thr^{475}	11	T475S
Thr^{478}	11	T478S and T478F

Cell Surface Targeting of Mutant Transporters—The observed changes in the uptake activity of a given mutant could be due to an alteration in its intrinsic transport capacity or to a disruption of its trafficking to the plasma membrane. To distinguish between these two circumstances, the mutant permeases that showed pronounced (>95%) loss of uptake (M40D, E157Q and E157D, F341A, G440F, and S469F and T478F), were tagged with GFP at the NH_2 terminus, and the corresponding genes were transfected into the transport defective Δ*ldnt1* background. Wild type LdNT1.1 was also GFP-tagged and served as control. Localization studies using direct GFP fluorescence microscopy demonstrated that the wild type LdNT1.1 permease was robustly synthesized and targeted to both the pellicular plasma membrane that surrounds the cell body and the flagellar pocket, an invagination of the plasma membrane located at the base of the flagellum (Fig. 3*A*). Importantly, all the mutants that showed a pronounced loss of transporter activity exhibited normal targeting to the pellicular plasma membrane and the flagellar pocket (Fig. 3, *B–H*), indicating that the loss of function is not caused by mistargeting or impaired trafficking to the cell surface but rather by a defect in the transport activity *per se*.

Analysis of Mutations Supports the ab Initio Structural Model for LdNT1.1—The current and previous mutational analyses allowed evaluation of the three original *ab initio* structures and selection of one preferred model for subsequent refining and validation. In many respects, the three models were in good agreement regarding their topology and the spatial arrangement of the TM helices. However, TM11 was predicted to be adjacent to the central cavity of the permease and between TM2 and TM7 by one of the three *ab initio* models (model 2) and by the threading model (Fig. 1*A*). In contrast, two of the *ab initio* models (models 1 and 3) placed TM11 at the periphery of the permease between TM7 and TM9. The negligible uptake values for mutants S469F and T478F, both located in TM11, supported the pore-lining location of TM11 in model 2 *versus* the more peripheral position of this helix in models 1 and 3 (Fig. 1*A*).

The preferred *ab initio* model 2 (Fig. 1, *B–G*) was then compared with an LdNT1.1 structural model computationally generated by threading analysis (Fig. 1, *H–M*), as previously described for LdNT2 (12). The overall similarity in helix packing for both structures (Fig. 1, *A*, *B*, *E*, *H*, and *K*), derived by distinct computational methods, reinforces the likelihood that these models represent a reasonably accurate helical bundling for this permease. Nonetheless, some of the mutagenesis data (such as residue Met^{40} (TM1), not included in the threading model because of its location outside the boundaries of putative TM1; residue Glu^{94} (TM2), outward-oriented in the threading model yet abrogating transport when mutated to Gln or Asp; or residue Arg^{378} (TM8), pore-oriented in the threading model despite playing a merely structural role) were better explained by the *ab initio* model.

Delineation of the Pore by Docking Analysis—To attempt to define the permeation pore of LdNT1.1, adenosine was "docked" (37, 38) to both the *ab initio* and the threading model. The positions of the adenosine from the top 100 docking solutions (Fig. 1, *D*, *G*, *J*, and *M*, *gray density*) were superimposed onto the models to predict the regions of the permease most likely to interact with adenosine. The *ab initio* model (Fig. 1, *D* and *G*) provided a more compact cluster of docked substrates than the threading model (Fig. 1, *J* and *M*), which contained multiple lobes of substrate clusters both within and below the plane of the membrane.

The ab Initio Model Predicts an Aromatic Interaction Motif—One test of the utility of a structural model is the ability to predict amino acids that play crucial roles in transport. The *ab initio* model of LdNT1.1 (Fig. 1, *B* and *E*) revealed that TM1, TM2, and TM7 cluster together at the extracellular face of the permease and largely close off the permeation pathway, similar to the arrangement of these same helices noted in the structure of the LacY permease in the inward facing orientation (28). Examination of these helices in the *ab initio* model of LdNT1.1 (Fig. 4) revealed a cluster of three aromatic amino acids, one from each helix (Phe^{48}, TM1; Trp^{75}, TM2; and Phe^{346}, TM7), that are predicted to be in close physical proximity to each other. These observations support the hypothesis that these

FIGURE 1. **Structural models of LdNT1.1 based on *ab initio* and threading analyses.** Helices are indicated by rigid cylinders and are numbered 1–11. Specific amino acid side chains are shown as space-filling models and are labeled with the corresponding residue designation. *A*, three hypothetical *ab initio* models for LdNT1.1 derived from Rosetta modeling are presented and compared with a model obtained by threading analysis upon the template of the 3-glycerol-phosphate transporter of *E. coli*. *B*, *C*, *E*, and *F* depict side and cytosolic views, respectively, of preferred *ab initio* model 2. *H*, *I*, *K*, and *L* depict side and cytosolic views, respectively, of the threading model. Residues whose mutation cripples transport are highlighted in *green*, residues whose mutation alters substrate specificity are colored in *red*, residues whose mutation disrupts trafficking to the cell surface are shown in *yellow*, and residues whose mutation produces moderate changes in transport activity are separately grouped (*C*, *F*, *I*, and *L*) and depicted in *blue*. Mutations in several residues highlighted here, Glu^{121} and Asp^{215} (9) and Thr^{186} and Val^{193} (13), were not reported elsewhere in this manuscript but were documented in the associated references. *D*, *G*, *J*, and *M* offer side and cytosolic views, respectively, of the docking of adenosine (*gray density*) into the *ab initio* (*D* and *G*) and threading models (*J* and *M*). The structures in this figure and in Fig. 4 were generated using PyMOL.

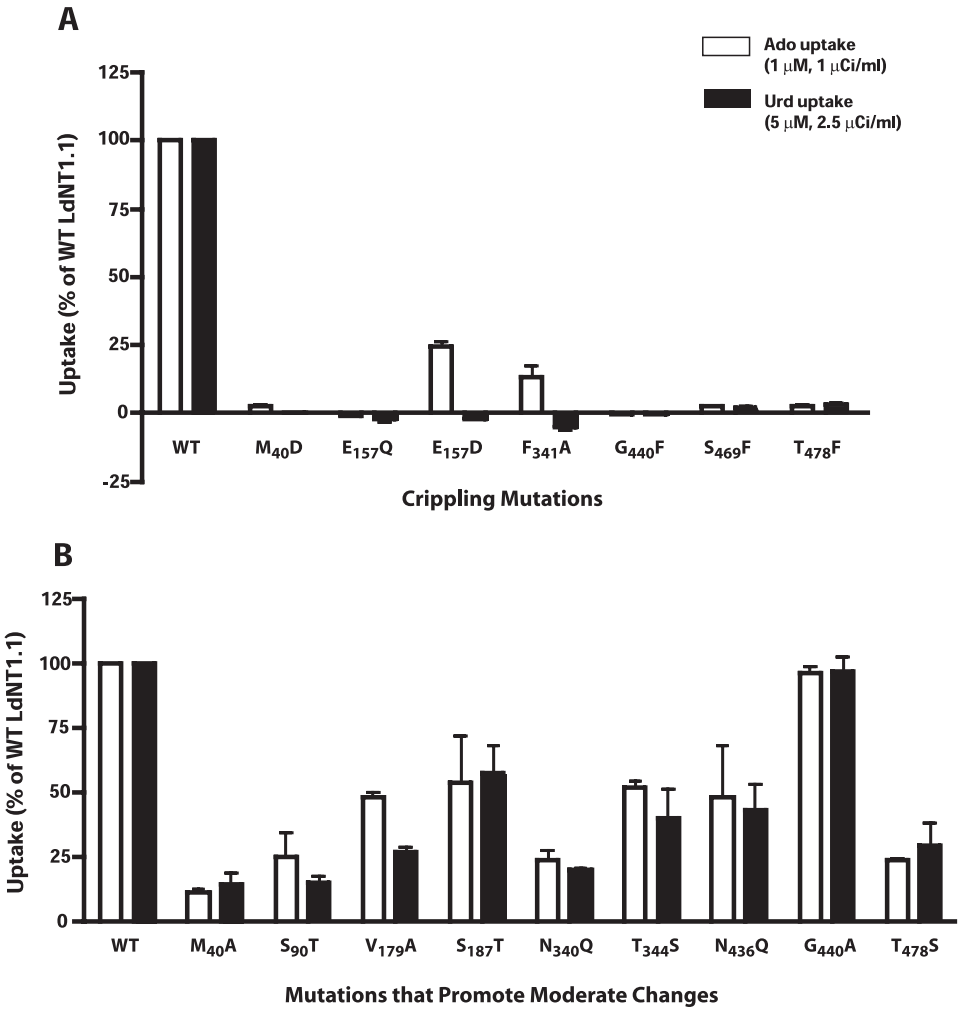

FIGURE 2. **Functional expression of LdNT1. 1 permeases with crippling mutations (*A*) or mutations that resulted in moderate but significant inhibition of transport activity (*B*).** Uptake of [^{3}H]adenosine (*Ado*) (1 μM, 30s) and [^{3}H]uridine (*Urd*) (5 μM, 30 s) were determined at room temperature (~22 °C) and expressed as percentages of the uptake by wild type LdNT1.1. The level of background binding was subtracted from each point by measuring the uptake of radiolabeled ligand by parasites treated with 1% formaldehyde. Transport results represent means ± standard deviations for three independent experiments. For each mutant, two independent clones were isolated and tested in parallel to confirm each result (data not shown).

aromatic side chains might interact with each other, possibly by stacking of the aromatic rings, to close the outward end of the permeation pathway in the inward facing conformation. Hence these aromatic residues may play an essential role in the mechanism of transport. To test this prediction, each residue was mutated to an alanine, and the transport function of each mutant permease was measured in the Δ*ldnt1*/Δ*ldnt2* background. Uptake assays for both adenosine and uridine revealed that the F48A and W75A mutants were inactive in transport (Fig. 5*A*), whereas the F346A mutant was still functional. Furthermore, the conservative mutations F48Y, W75F, and W75Y retained substantial transport function (Fig. 5*B*), consistent with the importance of aromatic residues at these locations. Alignments of the sequences for the four ENT family members in *L. donovani* and the 12 ENTs in the related kinetoplastid parasite *T. brucei* (www.genedb.org) reveal a relatively high degree of conservation for an aromatic or occasionally a hydrophobic residue in the position equivalent to Phe^{48} and complete conservation of tryptophan in the position equivalent to Trp^{75} (supplemental Fig. S2). In contrast, the position equivalent to Phe^{346}, the residue whose mutation to alanine did not affect transport

TABLE 2

Summary of mutants of LdNT1.1 that exhibit strong phenotypes

Crippled refers to a >95% loss of adenosine uptake activity upon mutation. PPM refers to the pellicular plasma membrane that surrounds the cell body. FPM refers to the flagellar pocket membrane at the base of the flagellum. The references refer to previously published data on mutants not examined in this study. Mutations D389N and R393L were studied in the guanosine/inosine/xanthosine transporter LdNT2 and correspond to conserved residues Asp^{374} and Arg^{378} in LdNT1.1.

Residue	TM domain	Mutation(s)	Results	Targeting
Met^{40}	1	M40D	Crippled	PPM and FPM
Phe^{48}	1	F48A	Crippled	PPM and FPM
		F48W	Crippled	
Trp^{75}	2	W75A	Crippled	PPM and FPM
Glu^{94}	2	E94Q and E94D	Crippled (9)	PPM and FPM
Lys^{153}	4	K153A	Crippled (9)	Partially impaired
		K153R	Change of substrate specificity (9)	PPM and FPM
Glu^{157}	4/edge	E157D	Change of substrate specificity	PPM and FPM
		E157Q	Crippled	PPM and FPM
Gly^{183}	5	G183D	Crippled (22)	PPM and FPM
		G183A	Change of substrate specificity (22)	
Cys^{337}	7	C337Y	Crippled (22)	PPM and FPM
Phe^{341}	7	F341A	Change of substrate specificity	PPM and FPM
Asp^{374}	8	D389N	Crippled (LdNT2 (12))	PPM
Arg^{378}	8	R393L	Crippled (LdNT2 (12))	Impaired
Arg^{404}	9	R404A	Crippled (9)	Impaired
Gly^{440}	10	G440F	Crippled	PPM and FPM
Ser^{469}	11	S469F	Crippled	PPM and FPM
Ser^{478}	11	S478F	Crippled	PPM and FPM

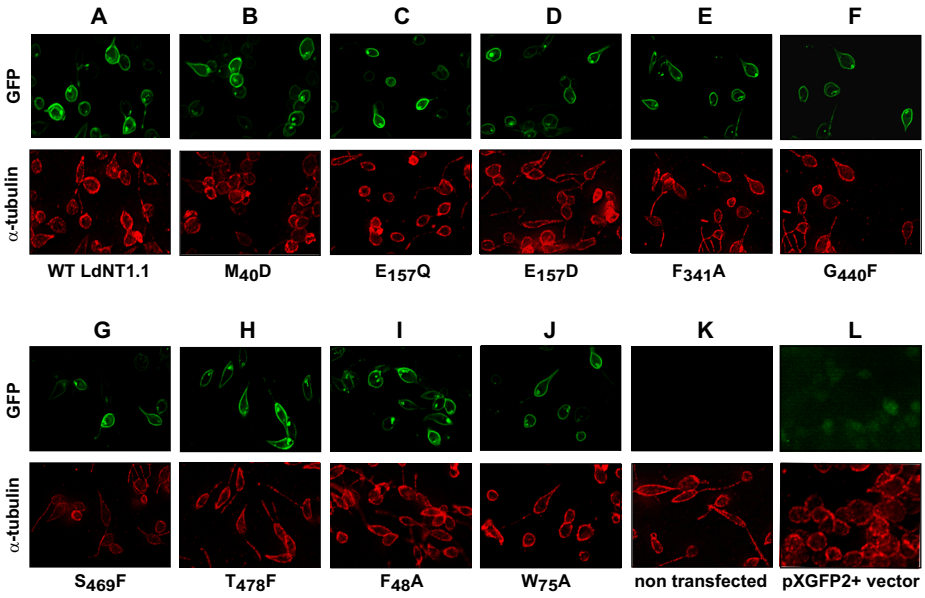

FIGURE 3. **Subcellular localization of LdNT1. 1 permeases containing crippling mutations.** Each mutant was expressed as a GFP fusion at the NH_2 terminus of the permease. Separate images are shown for GFP fluorescence (*top row*) and α-tubulin immunofluorescence (*bottom row*). Wild type LdNT1.1 permease was used as a positive control. Δ*ldnt1* parasites either not transfected (*K*) or transfected with the pXG-GFP+2′ vector that expresses unmodified GFP (*L*) were also used as controls.

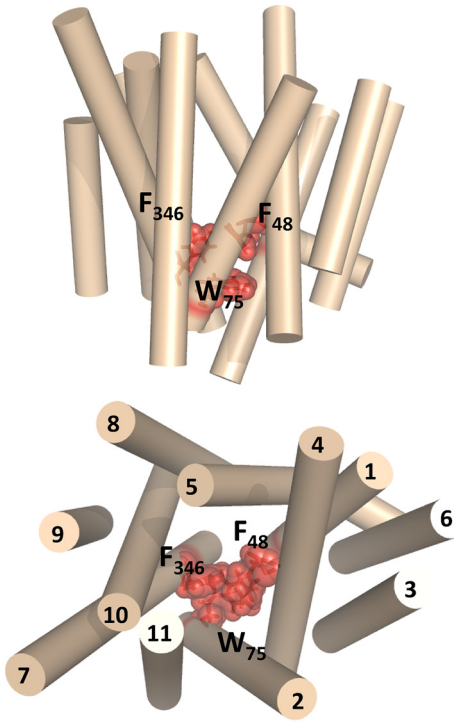

LdNT1.1 *ab initio* Model

FIGURE 4. **Proposed aromatic interaction motif.** Side (*top panel*) and cytosolic (*bottom panel*) view of the *ab initio* model of LdNT1.1 (helices shown in *tan*) showing a cluster of three aromatic residues (Phe^{48}, Trp^{75}, and Phe^{436}) that may interact to close an extracellular gate formed by TM1, TM2, and TM7. These three amino acids are indicated by stick and space-filling representations of the side chains.

activity, is not conserved and is a leucine in most of the kinetoplastid ENTs. Furthermore, as a negative control another highly conserved aromatic residue (Phe^{53}; supplemental Fig. S2) that is not predicted to be part of the aromatic interaction motif was mutated to an alanine. This F53A mutation did not significantly decrease transport activity (data not shown), demonstrating specificity for the affects of nonconservative mutations in residues Phe^{48} and Trp^{75}. Overall, these results support the hypothesis that at least two of the aromatic residues, Phe^{48} and Trp^{75}, may constitute an interaction motif or "aromatic clamp" required for the permease to assume the inward facing conformation. Because the F48A and W75A GFP-tagged mutants exhibited normal cell surface targeting (Fig. 3, *I* and *J*), the loss of function observed is attributable to an alteration in the intrinsic transport capability of the mutant permeases.

DISCUSSION

In the past few years, members of the ENT family of nucleoside and nucleobase transporters have garnered much attention because of their roles in metabolism and pharmacology related to cancer, heart disease and stroke, and infectious diseases (1). Recently, a tertiary topology model for the *L. donovani* inosine/guanosine/xanthosine permease LdNT2 was generated by threading analysis (12). This model proposed a packing of TM helices in LdNT2 similar to that determined from the crystal structure of the *E. coli* glycerol 3-phosphate transporter (39), a member of the major facilitator superfamily. Threading analysis of the *T. brucei* TbNBT1 nucleobase transporter modeled this permease upon the template of the LacY permease of *E. coli* (7), another member of the major facilitator superfamily. These two studies suggested that ENT family members may assume structures similar to major facilitator superfamily members, even though the two families of permease share no significant sequence identity.

Because a substantial body of experimental data on mutants of the related LdNT1.1 transporter is already available (9, 13, 22) that could be used to evaluate the accuracy of structural models, this permease was chosen to generate computational models. This approach employed Rosetta software (24–26), an informatics-based *ab initio* method that searches structures in the Protein Data Bank to predict the folding of each segment of the protein of interest, to generate a structural model of LdNT1.1. This method was chosen because it has been the most consistent and accurate in predicting the structures of folded domains in the critical assessment of techniques for protein structure predictions trials of modeling (40). In addition, the threading analysis was repeated to generate an alternate computational model of LdNT1.1. The application of two fundamentally different predictive algorithms allowed comparison of both models to

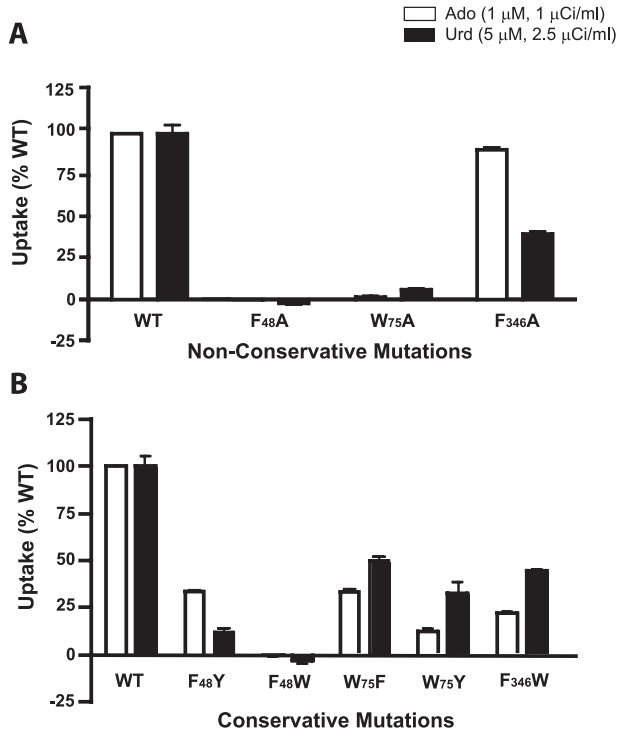

FIGURE 5. **Uptake by transporters with mutations in aromatic residues.** The results are shown for rates of [^{3}H]adenosine (*Ado*) and [^{3}H]uridine (*Urd*) uptake in the Δ*ldnt1*/Δ*ldnt2* cell line, using conditions reported in Fig. 2. *A*, uptake results for nonconservative alanine mutations. *B*, uptake results for conservative mutations. *WT*, wild type.

determine whether they generated similar or distinct structures for a single ENT family member.

The LdNT1.1 *ab initio* structure illustrated in Fig. 1 (*B*–*G*) is largely consistent with the modeling by threading analysis of LdNT2 (12) and LdNT1.1. (Fig. 1, *H*–*M*). In all cases, an inner bundle of TM helices (1, 2, 4, 5, 7, 8, 10, and 11) surrounds a hydrophilic cavity near the center of the bilayers. The other three TM helices (3, 6, and 9) are predicted to be peripheral to the central pore and face the surrounding membrane. The fact that such divergent computational approaches led to similar tertiary topologies provides additional confidence that the models offer a reasonable representation of helix packing for ENT permeases. The model presented here is also largely in agreement with threading analysis, employing the Lac permease as template, and mutagenesis performed by Papageorgiou *et al.* (7) using the *T. brucei* nucleobase permease TbNBT1. On the basis of their model and mutagenesis studies, these authors proposed that TM helices 5, 7, and 8 of TbNBT1 play important roles in transporter function, an observation consistent with the *ab initio* model of LdNT1.1 and the detection of critical residues in these helices of LdNT1.1 (Table 2). In addition, the similarities in *ab initio* and threading predictions for LdNT1.1 to the LacY and glycerol phosphate transporter structures further support the previously advanced hypothesis (7, 12) that ENT and major facilitator superfamily permeases share similar topologies, regardless of their low sequence similarity. Unanticipated similarities in the three-dimensional structures of transporters that belong to distinct families sharing minimal sequence similarity have been detected in recent crystal structure determinations. Thus the mammalian sodium-dependent glucose transporter SGLT1 (41), a member of the solute sodium symporter family, and a bacterial benzyl-hydantoin transporter (42), a member of the nucleobase cation symporter 1 (NCS1) family, have similar core structures to a bacterial leucine transporter LeuT (43), a member of the neurotransmitter sodium symporter family. Collectively, these studies reinforce the novel principle that distinct transporter families often assume similar helical packing topologies.

Nonetheless, we emphasize that some important distinctions exist between the *ab initio* and threading models of LdNT1.1. Thus residue Glu^{94}, whose mutation leads to crippling of transport activity (9), is predicted to line the permeation pathway in the *ab initio* model (Fig. 1*E*) but is oriented toward the membrane in the threading model (Fig. 1*K*). Similarly Met^{40} is not predicted to lie within a TM domain by the threading model; yet the M40D mutation abrogates transport activity. The potential interaction between the aromatic residues Phe^{48}, Trp^{75}, and Phe^{346} was predicted by the *ab initio* model (Fig. 4) but not by the threading model, in which TM1, TM2, and TM7 are not packed together as tightly (Fig. 1*K*) as in the *ab initio* model (Fig. 1*E*). Furthermore, the docking analysis for adenosine predicts a more compact pore using the *ab initio* approach (Fig. 1, *D* and *G*) than by threading analysis, where multiple lobes are apparent for the constellation of docked adenosines (Fig. 1, *J* and *M*). These results suggest that the *ab initio* model of LdNT1.1 may be a more accurate representation of transporter topology than the threading model.

In addition to comparing multiple computational approaches using a single permease, we also sought to evaluate the computational models using site-directed mutagenesis. A battery of new mutations was examined in the present study (Table 1), selected in part to help distinguish among the three initial *ab initio* models and between the *ab initio* and threading models. These studies allowed the identification of six new key residues whose mutation resulted in crippled transport activity (Met^{40}, Glu^{157}, Phe^{341}, Gly^{440}, Ser^{469}, and Thr^{478}) (Fig. 2*A*). Glu^{157} (near the cytoplasmic end of TM4) and Phe^{341} (within TM7) are of particular interest because the substitutions E157D and F341A resulted in transporters that exhibited a change in substrate specificity.

The present work also represents the first evidence of TM1, TM10, and TM11 participating in the permeation pathway through LdNT1.1, although former studies on human ENT1 and ENT2 already implicated helices 1 (10, 18) and 11 in inhibitor binding (11). Indeed, the rationale for generating the M40D (TM1), G440F (TM10), S469F (TM11), and T478F (TM11) mutants was that substitution of residues in these helices with bulky or charged amino acids would be likely to block the permeation pathway if TM1, TM10, and TM11 are pore-lining helices.

The observation that mutations that cripple transport activity or alter substrate specificity are predicted to cluster around the central pore (Fig. 1, *B*, *E*, *H*, and *K*) provides further experimental support consistent with the TM topology predicted by the two models. The strong transport phenotypes of these mutations would be explained most easily by a pore lining location. Furthermore, the tendency of mutations with modest effects on transport activity to assume peripheral locations in

the permease models also supports the TM helix arrangement proposed for both models (Fig. 1, *C*, *F*, *I*, and *L*). Perhaps the most interesting results to emerge from the *ab initio* model are those associated with mutagenesis of the aromatic residues Phe^{48}, Trp^{75}, and Phe^{346}. These residues were previously unknown to affect transport, but examination of the *ab initio* model suggested that they might interact to clamp TM1, TM2, and TM7 together in the inward facing conformation of the transporter. The observation that the F48A and W75A mutants are essentially devoid of transport activity is consistent with these two residues forming an interhelical interaction motif that is essential for the mechanism of transport. The observation that the F346A mutant retains transport activity could either indicate that Phe^{346} does not form part of the postulated interaction motif or that mutation of this residue is insufficient to destabilize the interhelical interactions.

These observations support the hypothesis that Phe^{48} and Trp^{75} contribute to the "alternating access" mechanism, believed to apply to many permeases including LacY (28), in which the transporter promotes migration of substrate across the membrane by alternately accessing an outward facing and inward facing conformation. It is notable that recent studies on the LacY permease, which assumes a helical topology (28) similar to that predicted for LdNT1.1, have revealed that TM1, TM2, and TM7 of that transporter form a periplasmic gate that closes the permeation pathway in the inward facing conformation but that opens up in the outward facing conformation (44). These observations suggest that both structural and mechanistic similarities may exist between LacY and LdNT1.1.

Despite the essential role for Phe^{48} in LdNT1.1, this residue is not conserved in the other three ENT family members from *L. donovani* (supplemental Fig. S2), suggesting that this residue does not serve the same essential function in all members of the ENT family among these parasites. The aromatic interaction proposed to occur in LdNT1.1 may be replaced by a distinct interaction, possibly involving other residues, in transporters such as LdNT2, LdNT3, and LdNT4. In contrast, this residue is conserved among most of the ENT family members from another kinetoplastid parasite *T. brucei* in which this residue is typically a Phe or Tyr. All of the family members in which Phe^{48} is conserved are adenosine transporters, with the exception of TbNT12.1, which transports adenine. This observation raises the possibility that the proposed aromatic clamp could be a determinant of substrate specificity.

The approach employed here entailed using multiple computational algorithms followed by evaluation of the resulting models by site-directed mutagenesis. The ability to make predictions about which residues are involved in transporter mechanism and to test such predictions experimentally, as we have done for the aromatic residues discussed above, demonstrates the inherent value of the *ab initio* model presented here. It is likely that the strategy of employing multiple computational approaches to derive structural models followed by testing these models by mutagenesis can be applied fruitfully for other permeases with unknown structures. We also expect that the *ab initio* model of LdNT1.1 will be useful for identifying other components of the permease that play central roles in transport function. Furthermore, this study underscores the ability of *ab initio* computation to provide valuable working models for the structures of polytopic membrane proteins as well as hydrophilic proteins, for which this methodology has been more commonly applied. Given the challenges of determining experimental structures for membrane proteins by x-ray crystallography or NMR, especially for permeases such as the ENTs that are not represented among bacteria, computational approaches provide a valuable alternative for pursuing structure-function studies on this important family of proteins.

Acknowledgments—We thank Marco Sanchez for performing the multi-alignment in supplemental Fig. S2 and Buddy Ullman for a critical reading of the manuscript.

REFERENCES

1. Kong, W., Engel, K., and Wang, J. (2004) *Curr. Drug Metab.* **5,** 63–84
2. Griffith, D. A., and Jarvis, S. M. (1996) *Biochim. Biophys. Acta* **1286,** 153–181
3. Carter, N. S., Yates, P., Arendt, C. S., Boitz, J. M., and Ullman, B. (2008) *Adv. Exp. Med. Biol.* **625,** 141–154
4. Murray, A. W. (1971) *Annu. Rev. Biochem.* **40,** 811–826
5. Rose, J. B., and Coe, I. R. (2008) *Physiology* **23,** 41–48
6. King, A. E., Ackley, M. A., Cass, C. E., Young, J. D., and Baldwin, S. A. (2006) *Trends Pharmacol. Sci.* **27,** 416–425
7. Papageorgiou, I., De Koning, H. P., Soteriadou, K., and Diallinas, G. (2008) *Int. J. Parasitol.* **38,** 641–653
8. Visser, F., Sun, L., Damaraju, V., Tackaberry, T., Peng, Y., Robins, M. J., Baldwin, S. A., Young, J. D., and Cass, C. E. (2007) *J. Biol. Chem.* **282,** 14148–14157
9. Valdés, R., Liu, W., Ullman, B., and Landfear, S. M. (2006) *J. Biol. Chem.* **281,** 22647–22655
10. Visser, F., Zhang, J., Raborn, R. T., Baldwin, S. A., Young, J. D., and Cass, C. E. (2005) *Mol. Pharmacol.* **67,** 1291–1298
11. Visser, F., Baldwin, S. A., Isaac, R. E., Young, J. D., and Cass, C. E. (2005) *J. Biol. Chem.* **280,** 11025–11034
12. Arastu-Kapur, S., Arendt, C. S., Purnat, T., Carter, N. S., and Ullman, B. (2005) *J. Biol. Chem.* **280,** 2213–2219
13. Valdés, R., Vasudevan, G., Conklin, D., and Landfear, S. M. (2004) *Biochemistry* **43,** 6793–6802
14. SenGupta, D. J., and Unadkat, J. D. (2004) *Biochem. Pharmacol.* **67,** 453–458
15. Arastu-Kapur, S., Ford, E., Ullman, B., and Carter, N. S. (2003) *J. Biol. Chem.* **278,** 33327–33333
16. Yao, S. Y., Ng, A. M., Vickers, M. F., Sundaram, M., Cass, C. E., Baldwin, S. A., and Young, J. D. (2002) *J. Biol. Chem.* **277,** 24938–24948
17. SenGupta, D. J., Lum, P. Y., Lai, Y., Shubochkina, E., Bakken, A. H., Schneider, G., and Unadkat, J. D. (2002) *Biochemistry* **41,** 1512–1519
18. Visser, F., Vickers, M. F., Ng, A. M., Baldwin, S. A., Young, J. D., and Cass, C. E. (2002) *J. Biol. Chem.* **277,** 395–401
19. Visser, F., Vickers, M. F., Zhang, J., Baldwin, S. A., Young, J. D., and Cass, C. E. (2002) *Biochem. Cell Biol.* **80,** 701–702
20. Yao, S. Y., Sundaram, M., Chomey, E. G., Cass, C. E., Baldwin, S. A., and Young, J. D. (2001) *Biochem. J.* **353,** 387–393
21. Sundaram, M., Yao, S. Y., Ng, A. M., Cass, C. E., Baldwin, S. A., and Young, J. D. (2001) *Biochemistry* **40,** 8146–8151
22. Vasudevan, G., Ullman, B., and Landfear, S. M. (2001) *Proc. Natl. Acad. Sci. U.S.A.* **98,** 6092–6097
23. Sundaram, M., Yao, S. Y., Ng, A. M., Griffiths, M., Cass, C. E., Baldwin, S. A., and Young, J. D. (1998) *J. Biol. Chem.* **273,** 21519–21525
24. Yarov-Yarovoy, V., Schonbrun, J., and Baker, D. (2006) *Proteins* **62,** 1010–1025
25. Bonneau, R., Strauss, C. E., Rohl, C. A., Chivian, D., Bradley, P., Malmstrom, L., Robertson, T., and Baker, D. (2002) *J. Mol. Biol.* **322,** 65–78

26. Simons, K. T., Kooperberg, C., Huang, E., and Baker, D. (1997) *J. Mol. Biol.* **268,** 209–225
27. Martí-Renom, M. A., Stuart, A. C., Fiser, A., Sánchez, R., Melo, F., and Sali, A. (2000) *Annu. Rev. Biophys. Biomol. Struct.* **29,** 291–325
28. Abramson, J., Smirnova, I., Kasho, V., Verner, G., Kaback, H. R., and Iwata, S. (2003) *Science* **301,** 610–615
29. Liu, W., Boitz, J. M., Galazka, J., Arendt, C. S., Carter, N. S., and Ullman, B. (2006) *Mol. Biochem. Parasitol* **150,** 300–307
30. Ha, D. S., Schwarz, J. K., Turco, S. J., and Beverley, S. M. (1996) *Mol. Biochem. Parasitol.* **77,** 57–64
31. LeBowitz, J. H. (1994) *Methods Cell Biol.* **45,** 65–78
32. LeBowitz, J. H., Coburn, C. M., McMahon-Pratt, D., and Beverley, S. M. (1990) *Proc. Natl. Acad. Sci. U.S.A.* **87,** 9736–9740
33. Vasudevan, G., Carter, N. S., Drew, M. E., Beverley, S. M., Sanchez, M. A., Seyfang, A., Ullman, B., and Landfear, S. M. (1998) *Proc. Natl. Acad. Sci. U.S.A.* **95,** 9873–9878
34. Jones, D. T. (1998) *FEBS Lett.* **423,** 281–285
35. Carter, N. S., Drew, M. E., Sanchez, M., Vasudevan, G., Landfear, S. M., and Ullman, B. (2000) *J. Biol. Chem.* **275,** 20935–20941
36. Sanchez, M. A., Tryon, R., Pierce, S., Vasudevan, G., and Landfear, S. M. (2004) *Mol. Membr. Biol.* **21,** 11–18
37. Brooijmans, N., and Kuntz, I. D. (2003) *Annu. Rev. Biophys. Biomol. Struct.* **32,** 335–373
38. Gschwend, D. A., Good, A. C., and Kuntz, I. D. (1996) *J. Mol. Recognit.* **9,** 175–186
39. Huang, Y., Lemieux, M. J., Song, J., Auer, M., and Wang, D. N. (2003) *Science* **301,** 616–620
40. Bradley, P., Malmström, L., Qian, B., Schonbrun, J., Chivian, D., Kim, D. E., Meiler, J., Misura, K. M., and Baker, D. (2005) *Proteins* **61,** (Suppl. 7) 128–134
41. Faham, S., Watanabe, A., Besserer, G. M., Cascio, D., Specht, A., Hirayama, B. A., Wright, E. M., and Abramson, J. (2008) *Science* **321,** 810–814
42. Weyand, S., Shimamura, T., Yajima, S., Suzuki, S., Mirza, O., Krusong, K., Carpenter, E. P., Rutherford, N. G., Hadden, J. M., O'Reilly, J., Ma, P., Saidijam, M., Patching, S. G., Hope, R. J., Norbertczak, H. T., Roach, P. C., Iwata, S., Henderson, P. J., and Cameron, A. D. (2008) *Science* **322,** 709–713
43. Yamashita, A., Singh, S. K., Kawate, T., Jin, Y., and Gouaux, E. (2005) *Nature* **437,** 215–223
44. Zhou, Y., Guan, L., Freites, J. A., and Kaback, H. R. (2008) *Proc. Natl. Acad. Sci. U.S.A.* **105,** 3774–3778